

Orbital periods of cataclysmic variables identified by the SDSS. V. VLT, NTT and Magellan observations of nine equatorial systems

John Southworth^{1*}, B. T. Gänsicke¹, T. R. Marsh¹, M. A. P. Torres², D. Steeghs^{1,2}, P. Hakala³, C. M. Copperwheat¹, A. Aungwerojwit^{1,4}, A. Mukadam⁵

¹ *Department of Physics, University of Warwick, Coventry, CV4 7AL, UK*

² *Harvard-Smithsonian Center for Astrophysics, 60 Garden Street, Cambridge, MA 02138, USA*

³ *Tuorla Observatory, University of Turku, FIN-21500 Piiikkiö, Finland*

⁴ *Department of Physics, Faculty of Science, Naresuan University, Phitsanulok, 65000, Thailand*

⁵ *Department of Astronomy, University of Washington, Box 351580, Seattle, WA 98195, USA*

16 November 2018

ABSTRACT

We present VLT and Magellan spectroscopy and NTT photometry of nine faint cataclysmic variables (CVs) which were spectroscopically identified by the Sloan Digital Sky Survey. We measure orbital periods for five of these from the velocity variations of the cores and wings of their H α emission lines. Four of the five have orbital periods shorter than the 2–3 hour period gap observed in the known population of CVs. SDSS J004335.14–003729.8 has an orbital period of $P_{\text{orb}} = 82.325 \pm 0.088$ min; Doppler maps show emission from the accretion disc, bright spot and the irradiated inner face of the secondary star. In its light curve we find a periodicity which may be attributable to pulsations of the white dwarf. SDSS J163722.21–001957.1 has $P_{\text{orb}} = 99.75 \pm 0.86$ min. By combining this new measurement with a published superhump period we estimate a mass ratio of $q \approx 0.16$ and infer the physical properties and orbital inclination of the system. For SDSS J164248.52+134751.4 we find $P_{\text{orb}} = 113.60 \pm 1.5$ min. The Doppler map of this CV shows an unusual brightness distribution in the accretion disc which would benefit from further observations. SDSS J165837.70+184727.4 had spectroscopic characteristics which were very different between the SDSS spectrum and our own VLT observations, despite only a small change in brightness. We measure $P_{\text{orb}} = 98.012 \pm 0.065$ min from its narrow H α emission line. Finally, SDSS J223843.84+010820.7 has a comparatively longer period of $P_{\text{orb}} = 194.30 \pm 0.16$ min. It contains a magnetic white dwarf and, with $g = 18.15$, is brighter than the other objects studied here. These results continue the trend for the fainter CVs identified by the SDSS to be almost exclusively shorter-period objects with low mass transfer rates.

Key words: stars: novae, cataclysmic variables – stars: binaries: close – stars: binaries: eclipsing – stars: binaries: spectroscopic – stars: white dwarfs – stars: dwarf novae

1 INTRODUCTION

Cataclysmic variables (CVs) are interacting binary stars containing a white dwarf primary component in a close orbit with a low-mass secondary star which fills its Roche lobe. In most of these systems the secondary component is hydrogen-

rich and transfers material to the white dwarf via an accretion disc. Comprehensive reviews of the properties of CVs have been given by Warner (1995) and Hellier (2001).

The evolution of CVs is thought to be governed primarily by the loss of orbital angular momentum due to gravitational radiation (Paczynski 1967) and magnetic braking (Verbunt & Zwaan 1981; Rappaport et al. 1982). These effects are predicted to cause CVs to evolve towards shorter orbital periods until a minimum value of about 80 min, at

* E-mail: j.k.taylor@warwick.ac.uk (JS),
Boris.Gaensicke@warwick.ac.uk (BTG),
T.R.Marsh@warwick.ac.uk (TRM)

which point the secondary stars become degenerate and the CVs evolve back to longer periods (e.g. Patterson 1998).

The distribution of orbital periods of the observed population of CVs has a characteristic ‘period gap’ (Whyte & Eggleton 1980; Knigge 2006) in the interval between 2.2 and 3.2 hours. The deficiency in the number of systems in this period range is thought to result from the sudden cessation of magnetic braking due to structural changes in CV secondary stars (Spruit & Ritter 1983). The number of CVs shortwards of this period gap are observed to be roughly equal to the number which are longward of the gap (e.g. Downes et al. 2001; Ritter & Kolb 2003).

Unfortunately, theoretical studies of the population of CVs have consistently predicted that the vast majority of these objects should have short periods ($P_{\text{orb}} \lesssim 2$ hours) due to their relatively longer evolutionary timescale (de Kool 1992; de Kool & Ritter 1993; Kolb 1993; Kolb & de Kool 1993; Politano 1996, 2004; Kolb & Baraffe 1999; Howell et al. 2001; Willems et al. 2005), culminating in a strong ‘spike’ in the population at a minimum period of about 65 min. The remarkable differences between the predicted and observed populations of CVs have not yet been satisfactorily explained, although it is clear that observational selection biases have a lot to answer for.

To understand these selection biases, and to discover what the properties of the intrinsic population of CVs are, we are conducting a research program to characterise the sample of CVs identified by the Sloan Digital Sky Survey (SDSS¹; York et al. 2000). A total of 212 of these objects have been found spectroscopically from an initial selection based on single-epoch photometric colour indices (Szkody et al. 2002, 2003, 2004, 2005, 2006, 2007). This sample is therefore not biased towards CVs which are variable or strong X-ray emitters, and also has a much wider coverage of colour space than previous large-scale surveys (Green et al. 1986; Chen et al. 2001; Aungwerojwit et al. 2006). Results and further discussion of our project to measure the orbital periods of SDSS CVs can be found in Gänsicke et al. (2006), Southworth et al. (2006, hereafter Paper I), Southworth et al. (2007a,b, 2008), Dillon et al. (2008a,b), and Littlefair et al. (2006a,b, 2007, 2008).

In this work we present time-resolved spectroscopy and photometry of nine CVs, and measure orbital period for five of these. We shall abbreviate the names of the targets to SDSS J0043, SDSS J0337, SDSS J1601, SDSS J1637, SDSS J1642, SDSS J1658, SDSS J1659, SDSS J2232 and SDSS J2238. Their full names and *ugriz* apparent magnitudes are given in Table 1. In Fig. 1 we have plotted their SDSS spectra for reference.

2 OBSERVATIONS AND DATA REDUCTION

A log of observations is given in Table 2. The reduced data and velocity measurements presented here will be made available at the CDS (<http://cdsweb.u-strasbg.fr/>) and at <http://www.astro.keele.ac.uk/~jkt/>.

¹ <http://www.sdss.org/>

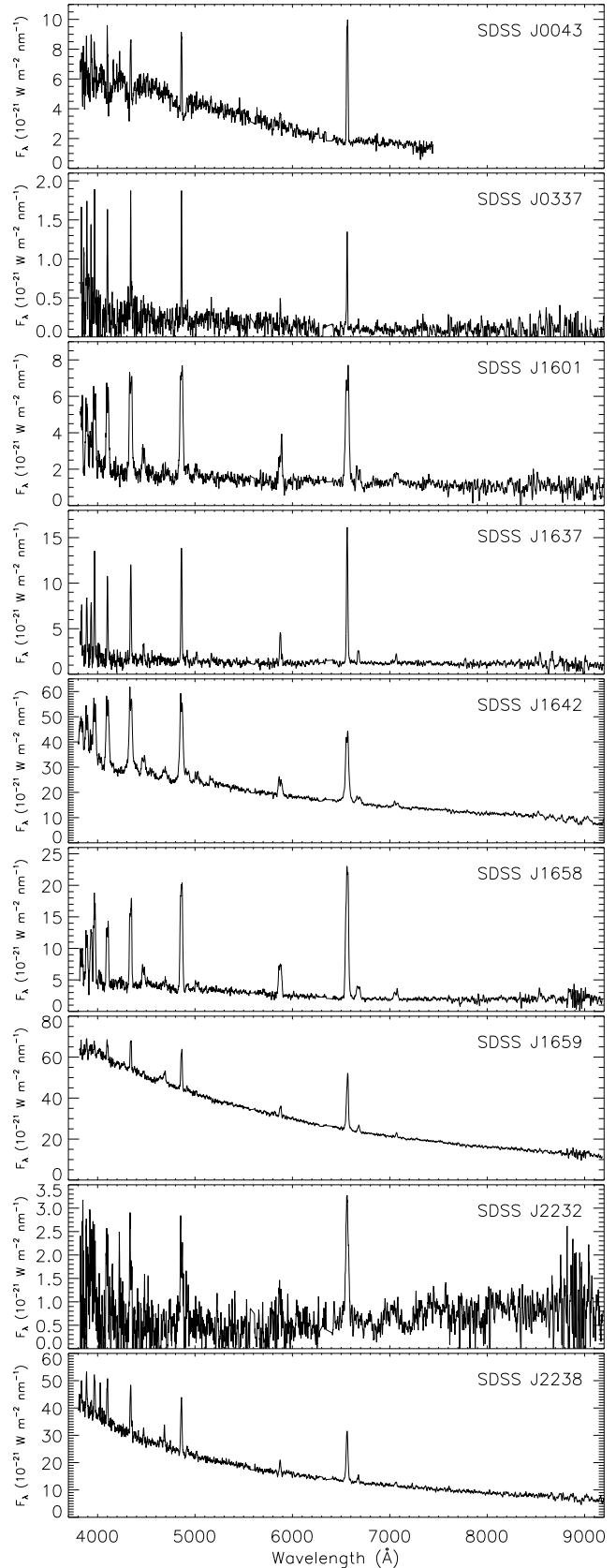


Figure 1. SDSS spectra of the CVs studied in this work. For this plot the flux levels have been smoothed with 10-pixel Savitsky-Golay filters. The units of the abscissae are $10^{-21} \text{ W m}^{-2} \text{ nm}^{-1}$, which corresponds to $10^{-17} \text{ erg s}^{-1} \text{ cm}^{-2} \text{ \AA}^{-1}$.

Table 1. Apparent magnitudes of our targets in the SDSS *ugriz* passbands. g_{spec} are apparent magnitudes we have calculated by convolving the SDSS flux-calibrated spectra with the *g* passband function. They are obtained at a different epoch to the *ugriz* magnitudes measured from the imaging observations, but are less reliable as they are affected by ‘slit losses’, and any errors in astrometry or positioning of the spectroscopic fibre entrance.

SDSS name	Short name	Reference	<i>u</i>	<i>g</i>	<i>r</i>	<i>i</i>	<i>z</i>	g_{spec}
SDSS J004335.14–003729.8	SDSS J0043	Szkody et al. (2004)	20.18	19.86	19.81	19.97	19.84	19.95
SDSS J033710.91–065059.4	SDSS J0337	Szkody et al. (2007)	19.64	19.54	19.72	19.97	20.14	23.27
SDSS J160111.53+091712.6	SDSS J1601	Szkody et al. (2006)	19.96	20.11	20.12	20.22	19.74	20.39
SDSS J163722.21–001957.1	SDSS J1637	Szkody et al. (2002)	16.83	16.60	16.59	16.75	16.84	20.57
SDSS J164248.52+134751.4	SDSS J1642	Szkody et al. (2007)	18.48	18.64	18.50	18.42	18.21	18.03
SDSS J165837.70+184727.4	SDSS J1658	Szkody et al. (2006)	20.51	20.07	20.12	20.09	19.68	19.71
SDSS J165951.68+192745.6	SDSS J1659	Szkody et al. (2006)	16.84	16.73	16.78	16.86	16.96	17.12
SDSS J223252.35+140353.0	SDSS J2232	Szkody et al. (2004)	17.74	17.66	17.80	17.88	17.97	23.16
SDSS J223843.84+010820.7	SDSS J2238	Szkody et al. (2003)	18.29	18.15	18.08	18.18	18.17	18.27

Table 2. Log of the observations presented in this work. The acquisition magnitudes were measured from the VLT/FORS2 acquisition images and are discussed in Section 2.2. The passbands for the acquisition magnitudes are indicated, where ‘*V*’ denotes the Johnson *V* band and ‘*Wh*’ indicates that no filter was used.

Target	Date (UT)	Start time (UT)	End time (UT)	Telescope and instrument	Optical element	Number of observations	Exposure time (s)	Mean magnitude
SDSS J0043	2007 08 16	07:47	10:25	VLT / FORS2	1200R grism	21	400	<i>V</i> = 19.9
SDSS J0043	2007 08 17	07:13	09:03	VLT / FORS2	1200R grism	14	440	<i>V</i> = 19.8
SDSS J0043	2005 10 08	05:05	06:49	APO 3.5m / DIS	unfiltered	175	15–20	<i>V</i> = 19.8
SDSS J0337	2007 08 17	09:20	10:18	VLT / FORS2	1200R grism	6	600	<i>V</i> = 21.4
SDSS J1601	2007 08 10	23:25	00:10	NTT / SUSI2	unfiltered	36	60	<i>Wh</i> = 20.1
SDSS J1637	2007 08 16	01:18	04:06	VLT / FORS2	1200R grism	20	600–400	<i>V</i> = 20.3
SDSS J1637	2007 08 16	23:28	00:40	VLT / FORS2	1200R grism	8	480	<i>V</i> = 20.6
SDSS J1642	2007 08 06	23:38	02:55	NTT / SUSI2	<i>V</i> filter	262	30	<i>V</i> = 19.5
SDSS J1642	2007 08 07	23:21	04:21	NTT / SUSI2	<i>V</i> filter	414	28	<i>V</i> = 19.6
SDSS J1642	2007 08 17	00:48	03:41	VLT / FORS2	1200R grism	29	300	<i>V</i> = 18.5
SDSS J1658	2007 08 15	00:17	03:23	VLT / FORS2	1200R grism	19	480	<i>Wh</i> = 19.5
SDSS J1658	2007 08 15	23:33	01:01	VLT / FORS2	1200R grism	12	400	<i>V</i> = 20.1
SDSS J1659	2007 08 11	00:19	02:45	NTT / SUSI2	<i>V</i> filter	166	30–60	<i>V</i> = 17.0
SDSS J2232	2005 08 11	00:10	05:34	NOT / ALFOSC	unfiltered	177	60	<i>Wh</i> = 22.1
SDSS J2232	2006 07 21	02:03	05:12	NOT / ALFOSC	unfiltered	109	60	<i>Wh</i> = 21.8
SDSS J2232	2007 08 15	03:37	06:10	VLT / FORS2	1200R grism	14	600	<i>V</i> = 21.4
SDSS J2238	2007 08 14	07:27	09:44	Magellan / IMACS	600 ℓ mm ^{−1} grism	22	300	
SDSS J2238	2007 08 15	07:24	09:51	Magellan / IMACS	600 ℓ mm ^{−1} grism	17	300	
SDSS J2238	2007 08 16	07:39	09:42	Magellan / IMACS	600 ℓ mm ^{−1} grism	19	300	

2.1 VLT spectroscopy

Spectroscopic observations were obtained in 2007 August using the FORS2 spectrograph (Appenzeller et al. 1998) and Very Large Telescope (VLT) at ESO Paranal, Chile. The 1200R grism was used for all observations, giving a wavelength interval of 5870 Å to 7370 Å with a reciprocal dispersion of 0.73 Å px^{−1}. From measurements of the full widths at half maximum (FWHMs) of arc-lamp and night-sky spectral emission lines, we estimate a resolution of 1.6 Å at H α .

1986) as implemented in the PAMELA² code (Marsh 1989), and the STARLINK³ packages FIGARO and KAPPA.

The wavelength calibration of the spectra was obtained using one arc spectrum per night, taken during daytime as part of the standard calibration routines for FORS2. As in Paper I we have found that flexure of the spectrograph can cause night-time spectra to shift by up to 42 km s^{−1} (1.2 pixels) depending on elevation. We have removed this trend from each spectrum by measuring the position of the OI night sky emission line at 6300.304 Å

² PAMELA and MOLLY were written by TRM and can be found at <http://www.warwick.ac.uk/go/trmarsh>

³ Starlink software can be accessed from <http://starlink.jach.hawaii.edu/>

The data were reduced using optimal extraction (Horne

(Osterbrock et al. 1996). Offsets calculated using other lines (e.g. O I 6363.78 Å) always agree to within 0.1 pixels.

The VLT spectra cover the H α and He I 6678 and 7065 Å lines. The average continuum-normalised H α profile for each object is plotted in Fig. 2.

2.2 VLT photometry

The observing procedure of FORS2 included obtaining target acquisition images. Exposure times were generally 20 s and the observations used either Johnson *V* or were unfiltered. We have extracted differential photometry from these images using the STARLINK package GAIA, taking special care to select comparison stars from the SDSS database with colours as close to our target CVs as possible in order to minimise colour effects. The *V*-band apparent magnitudes of the comparison stars were calculated from the *g* and *r* magnitudes using the transformations provided by Jester et al. (2005).

2.3 Magellan spectroscopy

Time-resolved spectroscopy of SDSS J2238 was obtained in 2007 August using the Inamori-Magellan Areal Camera and Spectrograph (IMACS; Bigelow & Dressler 2003) on the 6.5 m Magellan Baade Telescope at Las Campanas Observatory (Table 2). IMACS was employed in long-camera mode, using a 600 line mm⁻¹ grating centred at 5550 Å. This instrumental setup yielded a reciprocal dispersion of 0.76 Å px⁻¹ in the spectral interval 3920–7100 Å. The spectra were obtained dispersed along the short axis of four of the eight SITe CCDs in the IMACS mosaic detector. On August 14, most spectra were obtained with a 0.7 arcsec slit width which yielded a spectral resolution of 1.7 px (1.3 Å). The other data were obtained with a 1.2 arcsec slit width that provided a spectral resolution of 3.5 px (2.7 Å). Weather conditions during were generally good, with seeing ranging from 0.7'' to 1.2'' FWHM.

The IMACS frames were bias and flat-field corrected with standard IRAF routines. The spectra were extracted from each CCD frame with the IRAF KPNOSLIT package. The wavelength calibration was derived from cubic spline fits to HeNeAr lamp spectra bracketing the target spectra. The root mean square deviation of the fits was always less than 0.05 Å.

2.4 NTT photometry

SDSS J1601, SDSS J1642 and SDSS J1659 were observed using the New Technology Telescope (NTT) at ESO La Silla, Chile. Time-series imaging photometry was obtained using the SUSI2 high-resolution imager (D’Odorico et al. 1998). The observing run was affected by cloud, wind, snow and ice. For SDSS J1642 and SDSS J1659 we used a Johnson *V* filter. For SDSS J1601 we obtained unfiltered photometry and took care to avoid regions of the CCD where fringing was strong. The CCD was binned by factors of three in both directions, giving a spatial resolution of 0.24'' px⁻¹.

Debiasing and flat-fielding of the raw images was performed with the STARLINK software packages CONVERT and KAPPA. Optimal and aperture differential photometry

(Naylor 1998) was measured from the reduced images with the MULTIPHOTOM script (Southworth et al. 2004a), which uses the AUTOPHOTOM package (Eaton et al. 1999) to obtain time-series photometry. Differential magnitudes were converted into apparent magnitudes in way described in Section. 2.2.

2.5 NOT photometry

Light curves of SDSS J2232 were obtained in 2005 August and 2006 July using the Nordic Optical Telescope (NOT) and ALFOSC imaging spectrograph. The observations were unfiltered, windowed, and binned by a factor of 2 in both directions. The detector was an EEV 2k×4k pixel CCD with an unbinned plate scale of 0.19'' px⁻¹.

These data were reduced using the pipeline described by Gänsicke et al. (2004), which performs bias and flat-field corrections within MIDAS⁴ and uses the SEXTRACTOR package (Bertin & Arnouts 1996) to perform aperture photometry for all objects in the field of view. Differential magnitudes were converted into apparent magnitude in the same way as for our NTT and VLT photometry.

2.6 APO photometry

A light curve of SDSS J0043 was observed on 2005 October 8th using the 3.5 m telescope at Apache Peak Observatory (APO) and Dual Imaging Spectrograph (DIS) in imaging mode. With this instrument the blue and red portions of the beam are split by a dichroic at 5550 Å. We present here the blue-arm photometry, which is unfiltered but sensitive to light in the wavelength interval 3500–5550 Å. The CCD had a plate scale of 0.4 Å px⁻¹, and windowing was used to decrease the readout time. We used a standard IRAF reduction to extract sky-subtracted light curves from the CCD frames using weighted circular aperture photometry (O’Donoghue et al. 2000).

3 DATA ANALYSIS

3.1 Radial velocity measurement

We measured radial velocities (RVs) from emission lines in the spectra of our targets⁵ by cross-correlation with single and double Gaussian functions (Schneider & Young 1980; Shafter 1983), as implemented in MOLLY. In each case we tried a range of different widths and separations for the Gaussians in order to verify the consistency of our results (see Paper I for further details).

3.2 Orbital period measurement

The RVs and light curves for each CV were searched for periods using periodograms computed by the Scargle (1982) method, analysis of variance (AoV; Schwarzenberg-Czerny 1989) and orthogonal polynomials

⁴ <http://www.eso.org/projects/esomidas/>

⁵ The reduced spectra and RVs presented in this work will be available at the CDS (<http://cdsweb.u-strasbg.fr/>) and at <http://www.astro.keele.ac.uk/~jkt/>

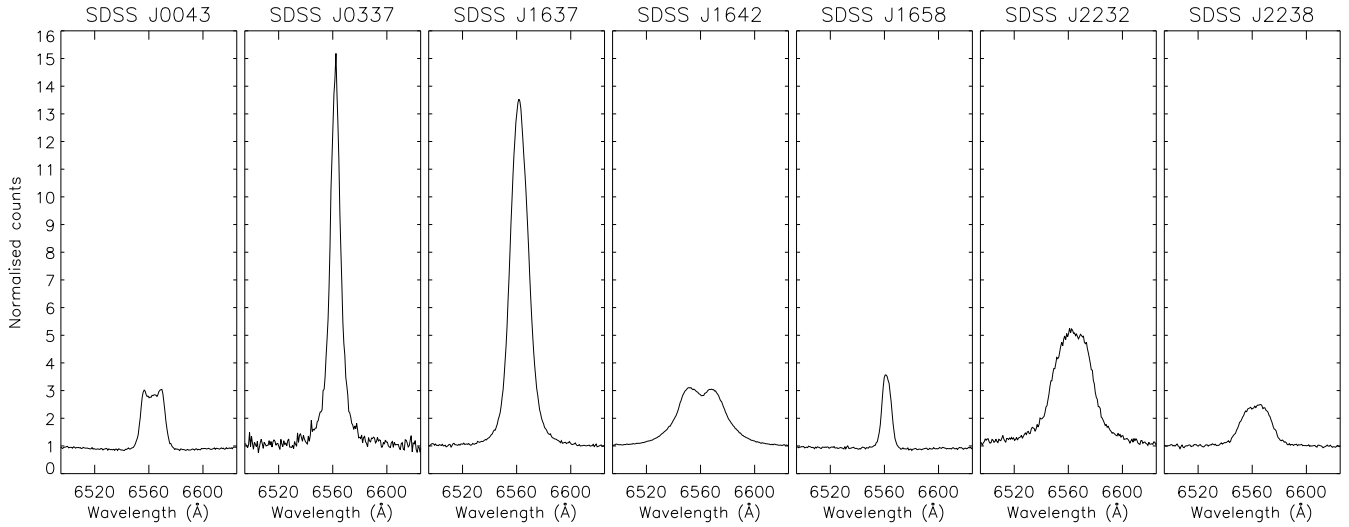


Figure 2. The averaged H α emission line profiles of the seven CVs for which we present spectroscopy. The spectra have had their continuum level normalised to unity. The orbital motion was removed from the spectra of SDSS J1658 before its mean spectrum was constructed.

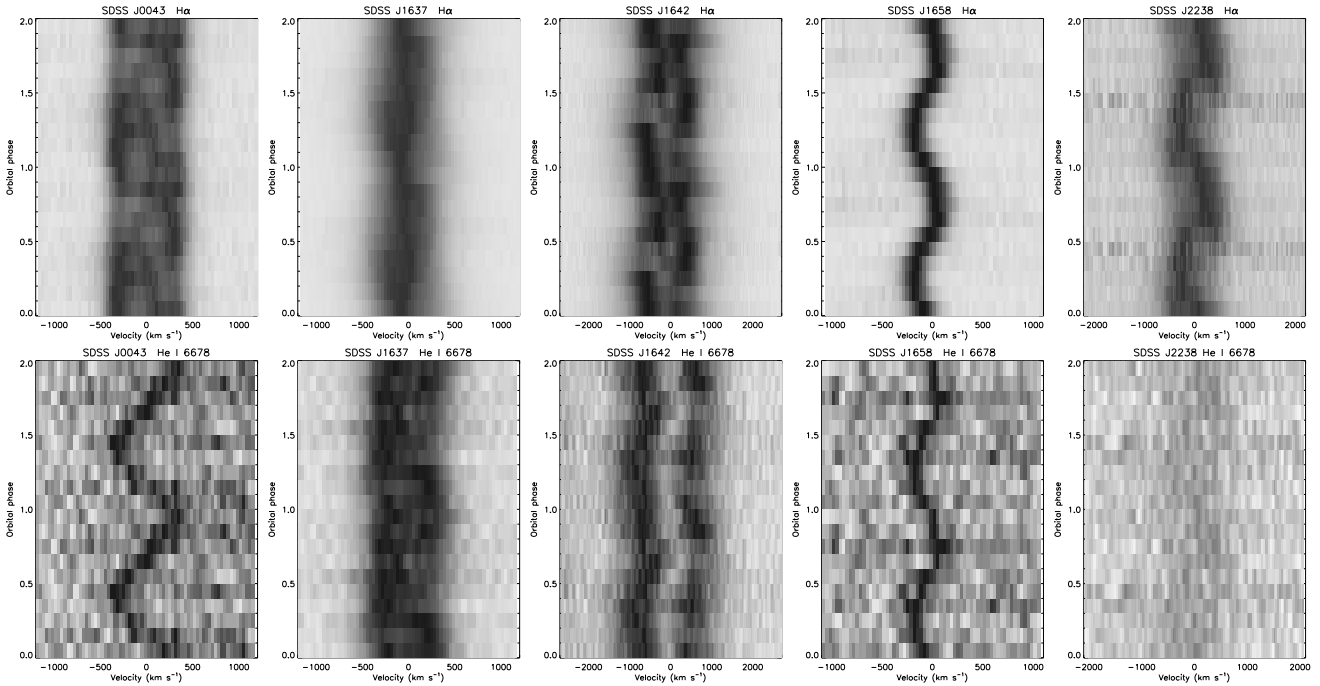


Figure 3. Greyscale plots of the continuum-normalised and phase-binned trailed spectra of the five CVs for which we obtained orbital periods. Darker shading indicates stronger emission. The upper plots show the H α lines. The lower plots show the He I 6678 Å lines, with the same velocity scale but different intensity scale. The He I spectra have been smoothed with a Savitsky-Golay filter for display purposes.

(ORT; Schwarzenberg-Czerny 1996), as implemented within the TSA⁶ context in MIDAS. In general two Fourier terms were used for ORT, which is appropriate for the relatively simple variation exhibited by these objects.

To find the final values of the orbital periods, and to investigate the aliases in the periodograms, we fitted circular spectroscopic orbits (sine curves) to the data using the

SBOP⁷ program, which we have previously found to give reliable error estimates (Southworth et al. 2005). The parameters of the final spectroscopic orbits are given in Table 3, and greyscale plots of the trailed spectra are shown in Fig. 3.

In some cases, to assess the likelihood of the point of highest power corresponding to the actual orbital period we

⁷ Spectroscopic Binary Orbit Program, written by P. B. Etzel,

⁶ [http://www.eso.org/projects/esomid/doc/user/98NOV/volb/nod420.html](http://www.eso.org/projects/esomid/2002/01/20020101/20020101.html), <http://www.mintaka.sdsu.edu/faculty/etzel/>

Table 3. Circular spectroscopic orbits found using SBOP. Phase zero corresponds to the blue-to-red crossing point of the RVs; because we are measuring emission lines from the accretion disc this usually has a phase offset with respect to inferior conjunction of the white dwarf (see Section 4.5).

Target	Orbital period (day)	Reference time (HJD)	Velocity amplitude (km s^{-1})	Systemic velocity (km s^{-1})	σ_{rms} (km s^{-1})
SDSS J0043	0.0571702 ± 0.000061	$2454328.87140 \pm 0.00071$	50.0 ± 2.8	13.1 ± 2.0	11.8
SDSS J1637	0.067391 ± 0.00013	2454326.6720 ± 0.0043	24.4 ± 1.6	-9.1 ± 1.2	6.0
SDSS J1642	0.07889 ± 0.0011	$2454329.55238 \pm 0.00074$	105.9 ± 2.4	-55.1 ± 2.4	12.7
SDSS J1658	0.0680638 ± 0.000045	$2454327.54703 \pm 0.00037$	125.3 ± 3.5	-41.5 ± 2.4	13.5
SDSS J2238	0.134932 ± 0.00011	2454326.8701 ± 0.0013	170.7 ± 5.1	-23.0 ± 4.0	27.3

have performed bootstrapping simulations (see Paper I) by randomly resampling the data with replacement and calculating a new periodogram a total of 1000 times (Press et al. 1992, p. 686). The fraction of periodograms in which the highest peak fell close to a particular alias can be interpreted as the likelihood of that alias being correct. However, in these cases we expect the resulting probabilities for the correct peak to be quite conservative (i.e. too low) for two reasons. Firstly, because the simulated datasets necessarily contain fewer unique epochs than the original data some temporal definition is sacrificed. The bootstrapping periodograms are often clearly inferior to those calculated from the actual data, confirming this picture. Secondly, when picking the best alias interactively we use more information than just the periodogram (including the shape of the phased radial RV curve).

At the suggestion of the referee we have also performed Monte Carlo simulations, using the same approach as in Southworth et al. (2004b,c). These have the advantage that they do not suffer from a loss of time information, but the drawback that a sine curve is assumed to be a good representation of the data. This is not always the case for CVs, which often has substantial non-Keplerian kinematical effects. We find, as expected, that Monte Carlo simulations generally give a higher significance level (by a factor of two in percentage terms) to the highest peak in a periodogram.

4 RESULTS FOR EACH SYSTEM

4.1 SDSS J004335.14–003729.8

SDSS J0043 was found to be a CV by Szkody et al. (2004) from an SDSS spectrum which shows a blue continuum with narrow Balmer emission lines. There are very broad Balmer absorption lines attributable to the white dwarf component of the system, but no identifiable features arising from the secondary star. Szkody et al. (2004) obtained nine low-resolution spectra of SDSS J0043 over 2.7 h using the 3.5 m telescope and Double Beam Spectrograph at Apache Point Observatory (APO). RVs from the H α and H β emission lines yielded orbital periods of about 1.5 h and 1.2 h, respectively.

We obtained a total of 35 VLT spectra of SDSS J0043 (21 on one night and 14 on the next night). The H α line is relatively narrow (about 1000 km s^{-1}) but is clearly double-peaked and variable (Fig. 2). RV measurements consistently give orbital periods close to 82 min, and the best results are found using a single Gaussian of width 1500 km s^{-1} . Data

from the first night alone give $P_{\text{orb}} = 82.4 \pm 2.4$ min. Including the spectra from the second night too gives $P_{\text{orb}} = 82.325 \pm 0.088$ min. The adjacent one-day aliases at 77.75 and 87.49 min differ from the first-night period by 2σ , so are unlikely to be correct but cannot be ruled out. Bootstrapping simulations (which we expect to be conservative) give a probability of 75% that we have identified the orbital period correctly, and respectively 6% and 19% that the peaks at 77.75 and 87.49 min are actually the orbital period. Monte Carlo simulations give a probability of 89% for this period, and probabilities of 2% and 9% for the other peaks. The parameters of the final spectroscopic orbit are given in Table 3 and the orbit and Scargle periodogram are plotted in Fig. 4.

A diagram of the phase-binned trailed spectra of SDSS J0043 shows that the relative strengths of the double peaks is variable (Fig. 3) and that there is emission in the form of an S-wave from the bright spot on the edge of the accretion disc (Smak 1985). The He I 6678 Å emission line is narrow and single-peaked (Fig. 3) and has the same phasing as the emission from the bright spot in H α .

4.1.1 Photometry of SDSS J0043: does it contain a pulsating white dwarf?

Fig. 5 shows the light curve we have obtained of SDSS J0043. A periodogram of these data shows a peak at a frequency near to 400 cycle d^{-1} . A fit to this peak results in a period of 207 ± 1 s and an amplitude of 17 ± 5 mmag. This period is within the range of values typically exhibited by ZZ Ceti stars (pulsating white dwarfs), but the amplitude is large for this type of star (Winget 1998; Mukadam et al. 2004). These observations therefore suggest that the white dwarf in SDSS J0043 is a ZZ Ceti star. More extensive data are needed for confirmation.

4.1.2 Doppler tomography of SDSS J0043

The complexity of the H α emission line observed for SDSS J0043 prompted us to decompose the emission into velocity space using Doppler tomography. A Doppler map of this line was computed using the maximum entropy method (Marsh & Horne 1988) and is shown in Fig. 6. The χ^2 value for the Doppler map was chosen to be marginally larger than the value for which noise features start to be visible. SDSS J0043 is not eclipsing, so the exact orientation of the map is not known. The velocity modulation of emission lines from the accretion discs of CVs are habitually

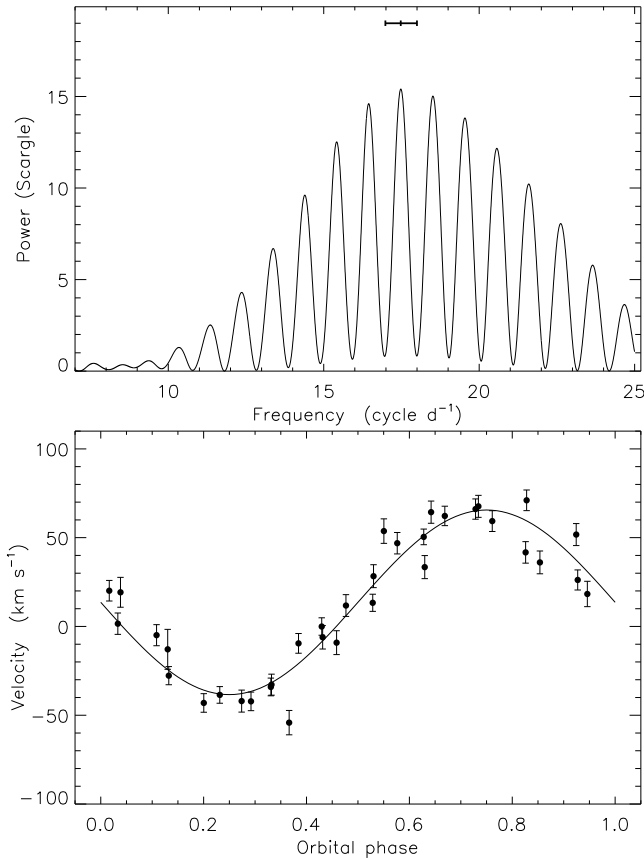


Figure 4. *Upper panel:* Scargle periodogram of the RVs of SDSS J0043 measured using a single Gaussian with width 1500 km s^{-1} . The measured period and uncertainty from data from the first night only are indicated with an error bar at the top of the plot. *Lower panel:* measured RVs (filled circles) compared to the best-fitting spectroscopic orbit (solid line).

offset in phase from the true motion of the white dwarf (e.g. Stover 1981; Steeghs et al. 2007). We therefore adopted the spectroscopic orbit and experimented with phase offsets of 0.10–0.25, a range which covers the values found in most studies of eclipsing CVs. The best-fitting calculated spectra and residuals are shown in Fig. 7.

The Doppler map in Fig. 6 shows a circular emission feature at large velocities which comes from the accretion disc of SDSS J0043. There is no emission at low velocities which could be attributed to the white dwarf. However, there is an emission peak at $(V_X, V_Y) = (100, 0)$ which may arise from the irradiated inner face of the secondary star. We have overplotted several features on the Doppler map to illustrate this interpretation. The Roche lobe of the secondary is shown with a solid line, the centres of mass of the system and of the two stars are shown by crosses, and the velocity of the accretion stream and the Keplerian velocity of the accretion disc are indicated by dots with a constant spacing in position. We have adopted $K_{\text{WD}} = 50 \text{ km s}^{-1}$ for the white dwarf velocity amplitude (Table 3). To position the inner Lagrangian point of the secondary on the emission peak we used a phase offset of 0.21 (corresponding to a clockwise rotation of the map of 76°) and a secondary star velocity amplitude of $K_2 = 200 \text{ km s}^{-1}$. This interpretation leads to

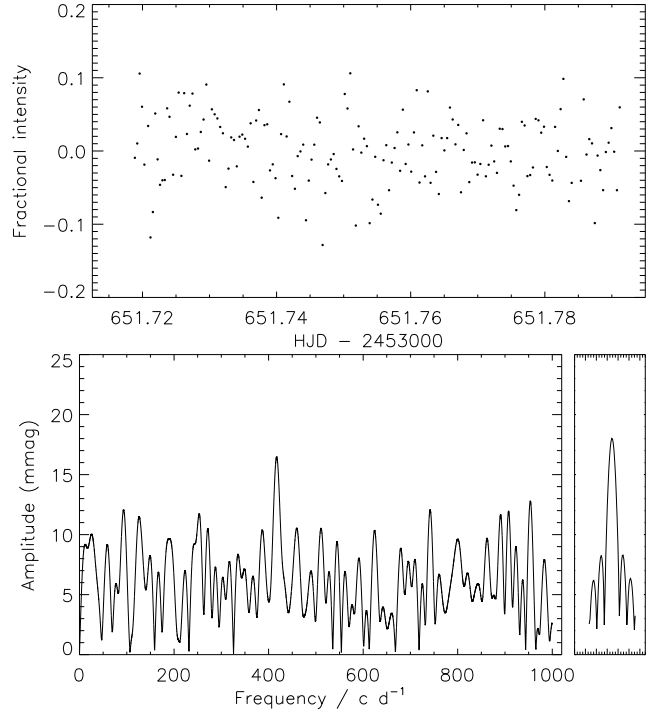


Figure 5. *Upper panel:* Light curve of SDSS J0043 given as fractional change in intensity. *Lower panels:* Amplitude spectrum of the light curve (left) and the window function (right).

a mass ratio of $q = \frac{M_2}{M_{\text{WD}}} = 0.25$, which is larger than expected and unlikely to be real. We discuss this further below.

The accretion disc has two regions of enhanced emission in the Doppler map. The one at $(V_X, V_Y) = (-350, 100)$ is in the path of the accretion stream from the secondary star’s surface at the inner Lagrangian point, supporting our interpretation of the map. Doppler maps of helium emission can be useful indicators of the velocity of this bright spot, so a map of the He I 6678 \AA emission was constructed (not shown) using the same procedure as for the $\text{H}\alpha$ map. This displays only one significant feature: a spot of emission centred on roughly $(V_X, V_Y) = (-250, 150)$ which confirms that this emission region is arising from the bright spot in SDSS J0043.

The second region of enhanced emission from the accretion disc, at $(V_X, V_Y) = (-100, -350)$, is not a typical feature of Doppler maps of CV emission lines. This has no immediate explanation in the accepted picture of the structure of short-period CVs, but has previously been seen in some AM CVn system (e.g. Roelofs et al. 2006). A second oddity for this system is that the placement of the inner emission feature on the substellar point of the secondary star required $K_2 = 200 \text{ km s}^{-1}$, which with $K_{\text{WD}} = 50 \text{ km s}^{-1}$ results in $q = 0.25$, much larger than the expected value of $q \sim 0.1$ for a CV with $P_{\text{orb}} = 82 \text{ min}$ (Knigge 2006). The latter difficulty could be explained by the former: the region of enhanced emission at $(V_X, V_Y) = (-100, 350)$ will distort the $\text{H}\alpha$ profiles and thus the velocities measured from them. The spectroscopic orbit measured above is therefore unlikely to accurately represent the motion of the white dwarf. This caveat is supported by the phase difference of 0.21 between

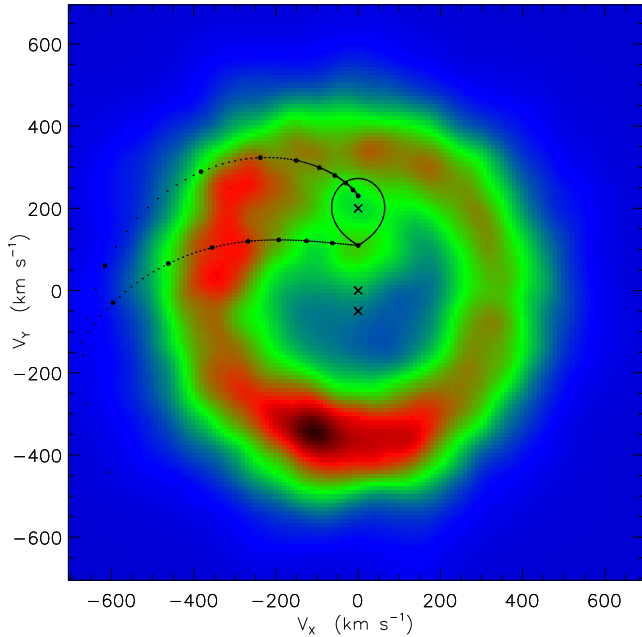


Figure 6. Doppler map of the $H\alpha$ emission line from SDSS J0043. Strong emission is coloured red and weak to no emission is blue. The Roche lobe of the mass donor is indicated by a solid curve, and the centre of mass of the system and individual stars are shown with crosses. The dots indicate the velocity of the accretion stream and the Keplerian velocity of the disc along the path of the stream. They are positioned at every $0.01R_{\text{RL}}$, decreasing from $R_{\text{RL}} = 1.0$ at the mass donor, where R_{RL} is the radius of the Roche lobe of the white dwarf.

the spectroscopic orbit we measured from the $H\alpha$ emission and the velocity variation of the irradiated face of the secondary star, which in our experience is on the large side for short-period CVs. If K_{WD} were only 25 km s^{-1} then the mass ratio would become roughly $q = 0.12$, which is a reasonable value for this system. An alternative explanation is that the degenerate component has a low mass of $M_{\text{WD}} \sim 0.4 M_{\odot}$, which would make it a helium-core white dwarf.

4.2 SDSS J033710.91–065059.4

A spectrum of SDSS J0337 was presented by Szkody et al. (2007) which identified it as a CV with narrow Balmer emission lines. The apparent magnitude of SDSS J0337 was much brighter when it was observed during the SDSS imaging observations ($g = 19.54$) than when the SDSS spectrum was subsequently acquired ($g_{\text{spec}} = 23.3$). This is probably due to the system being in a higher state during the imaging observations, an explanation which is supported by the brightness of SDSS J0337 in our acquisition image ($V \approx 21.4$) being midway between the two SDSS magnitudes.

SDSS J0337 was the last object studied during our VLT observing run, and there was only time to obtain seven spectra over one hour. These show a sharp $H\alpha$ emission line (Fig. 2) with a FWHM of only about 500 km s^{-1} , with weaker narrow He I emission lines at 5876 \AA , 6678 \AA and 7065 \AA . We cannot detect any RV motion in the $H\alpha$ line, to an upper limit of 15 km s^{-1} . The narrow emission lines and

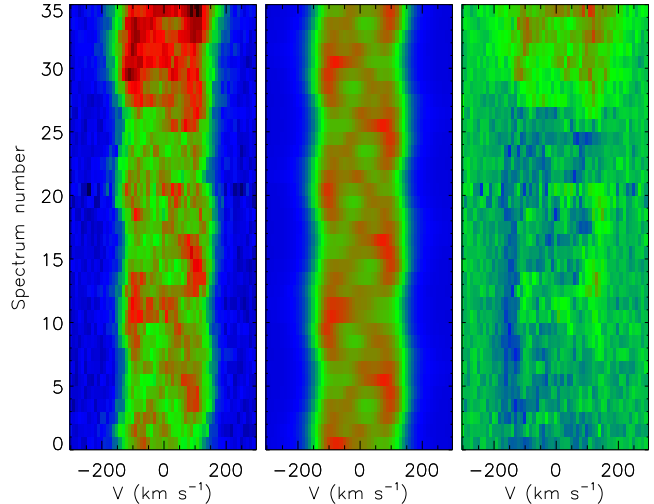


Figure 7. Comparison between the 35 observed spectra (left panel) and the best-fitting representation for the Doppler map (centre). The residuals (right) are shown in the right-hand panel.

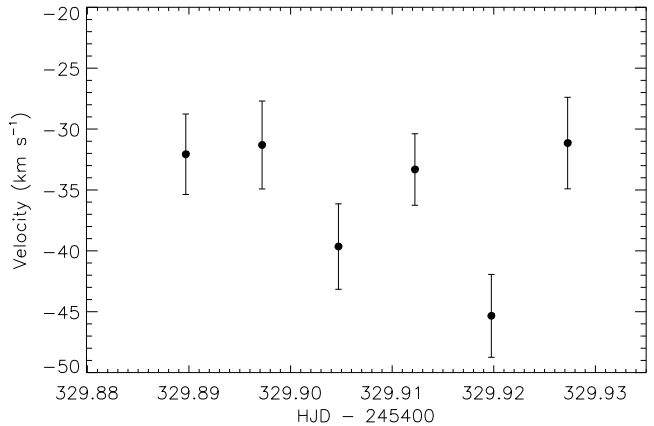


Figure 8. RVs measured for SDSS J0337 by cross-correlation against a single Gaussian function with FWHM 600 km s^{-1} .

lack of observable RV variation are consistent with a low orbital inclination for the SDSS J0337 system. A plot of its RVs, measured using a single Gaussian of width 600 km s^{-1} , is shown in Fig. 8. Obtaining the orbital period of this object may take a substantial amount of telescope time.

4.3 SDSS J160111.53+091712.6

SDSS J1601 was discovered to be a CV by Szkody et al. (2006) and has a spectrum characterised by strong Balmer and weak He I emission lines which are slightly double-peaked (Fig. 1). We obtained 45 min of NTT unfiltered photometry, which shows a variation of amplitude about $0.2\text{--}0.3 \text{ mag}$ (Fig. 9). The mean magnitude is consistent with the SDSS imaging and spectroscopic values. The variation is suggestive of a sinusoidal variation with a period similar to the duration of the observations. Further photometry of SDSS J1601 has a good chance of yielding a measurement of the orbital period of this binary.

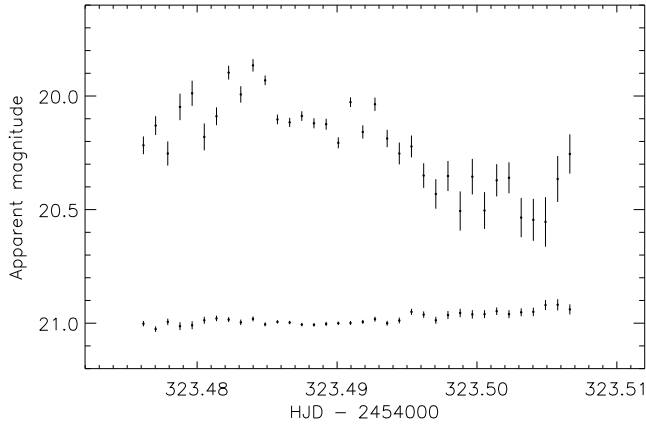


Figure 9. NTT unfiltered photometry of SDSS J1601. The magnitudes are differential with respect to a comparison star and have been offset by the r magnitude of the comparison star. Differential magnitudes for the comparison minus check stars are shown offset by +21.3 mag.

4.4 SDSS J163722.21–001957.1

SDSS J1637 is a faint CV ($V \approx 20.5$) which was in a high state when observed by the SDSS imaging survey ($g = 16.60$). The flux level of its SDSS spectrum (Szkody et al. 2002) ($g_{\text{spec}} = 20.6$) is similar to its apparent magnitude in our VLT acquisition observations ($V = 20.3$ and 20.6). Szkody et al. (2002) observed the system several times (the exact number is not given) and found it at 20th magnitude each time. A superoutburst of SDSS J1637 was observed by G. Bolt⁸ with a mean magnitude of $V \approx 15.5$ on the night of 2004 March 28. A superhump period of 0.06927 ± 0.0006 d (99.75 ± 0.86 min) was measured by G. Bolt from CCD photometry⁹.

We obtained 28 VLT spectra of SDSS J1637 over two nights, 20 of which were taken over three hours on the first night. These show a strong H α emission line with FWHM of only about 800 km s^{-1} , and much weaker He I emission at 6678 \AA and 7065 \AA . RV measurements with both single and double Gaussians of various widths are in good agreement with each other, and formally the best results are obtained using a single Gaussian of FWHM 500 km s^{-1} . RV measurements from the first night yield a period of 98.2 ± 2.1 min. Adding in the second night gives a best period of 97.0 min with one-day aliases at 90.2 and 104.9 min. Using the measurements from the first night to select the best alias gives an orbital period of 97.04 ± 0.19 min (Fig. 10). Bootstrapping simulations give a (conservative) probability of 80% that the orbital period refers to the 97-min peak in the periodogram, and a 19% probability that the 105-min alias is actually the correct period. Monte Carlo simulations are more confident, yielding an 88% probability for the 97-min peak and a 10% probability for the 105-min alias. The 97-min period receives further support from the observed superhump period for SDSS J1637, so can be unambiguously assigned to the orbital period of the system.

⁸ vsnet-superoutburst alert number 2306

⁹ vsnet-superoutburst alert number 2310

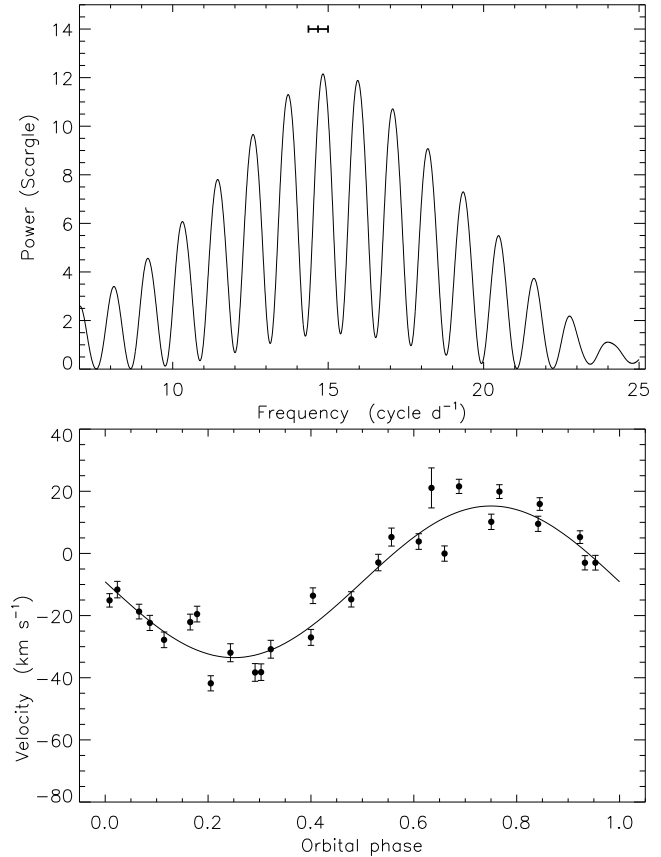


Figure 10. *Upper panel:* Scargle periodogram of the RVs of SDSS J1637 measured using a single Gaussian with width 500 km s^{-1} . The measured period and uncertainty from data from the first night only are indicated with a thick line. *Lower panel:* measured RVs (filled circles) compared to the best-fitting spectroscopic orbit (solid line).

4.4.1 The physical properties of SDSS J1637

There is strong evidence that the superhumps observed in CVs during superoutburst arise from the precession of an elliptical accretion disc (Vogt 1982; Whitehurst 1988), where the superhump period is the beat period between the orbital and precession periods. The ratio of the orbital and superhump periods is observed to depend on mass ratio in CVs (Patterson 1998), allowing the physical properties of SDSS J1637 to be estimated.

From measurements of the orbital and superhump periods of SDSS J1637 we find a superhump period excess (Patterson 1998) of $\epsilon(q) = 0.028 \pm 0.009$. Using the calibration presented by Patterson (1998) we obtain from this $q = 0.167$. The updated calibration given by Knigge (2006) results in $q = 0.161 \pm 0.037$, which is in agreement (but remember that the different calibrations have many objects in common). Estimating a white dwarf mass of $M_{\text{WD}} = 0.8 M_{\odot}$ (Smith & Dhillon 1998; Littlefair et al. 2008) results in a secondary star mass of $M_2 = 0.13 M_{\odot}$, in agreement with the properties of the semi-empirical CV secondary star sequence presented by Knigge (2006).

The measured spectroscopic orbit for SDSS J1637 has a low velocity amplitude of only $24.4 \pm 1.6 \text{ km s}^{-1}$ (Ta-

ble3). The phase-binned and trailed $H\alpha$ and HeI 6678 Å spectra show no large variation with orbital phase (Fig. 3). SDSS J1637 has the largest $H\alpha$ and HeI emission line equivalent widths of all of the objects we have studied with the VLT, which points to a very weak continuum. The $H\alpha$ emission line is strong, narrow and single-peaked. These results suggest that the SDSS J1637 binary system has a relatively low orbital inclination when observed from Earth. If the masses of the white dwarf and secondary star are $0.8 M_{\odot}$ and $0.13 M_{\odot}$ (see above), the velocity amplitude we have measured implies an orbital inclination of roughly 40° .

4.5 SDSS J164248.52+134751.4

SDSS J1642 was discovered to be a CV by Szkody et al. (2007) and has double-peaked Balmer and HeI emission lines. Weak emission at HeII 4686 Å is also visible in the SDSS spectrum. Szkody et al. (2007) presented seven low-resolution APO 3.5 m telescope spectra taken over an 80 min period and estimated an orbital period (70 ± 7 min, which is close to the duration of the observations) from RV measurements of the $H\alpha$ and $H\beta$ lines.

We obtained eight hours of V -filter photometry of SDSS J1642 over two nights in 2007 August using the NTT and SUSI2 imager. Exposure times of 30 s were used, giving an observing cadence of 43 s. This object is quite variable in brightness: it was at magnitude $g = 18.64$ in the SDSS imaging data, $g_{\text{spec}} = 18.0$ during its SDSS spectrum, averaging $V = 19.5$ on the night of 2007 August 06, and during the next night increased from $V = 19.8$ to $V = 19.3$ over five hours. Its apparent magnitude on our VLT acquisition image on the night of 2007 August 17 was $V = 18.5$.

The light curves from the two NTT nights are shown in Fig. 11. Periodic variation is seen during both nights, as well as a steady increase in brightness over the second night and quite a lot of flickering (Bruch 1992, 2000). Scargle periodograms show a small forest of peaks in the region between zero and 15 cycles per day (Fig. 11, panel 3) and it is not clear for these data if any of the peaks relates to the orbital period.

We observed SDSS J1642 for three hours with VLT/FORS2 on the night of 2007 August 17, obtaining 29 spectra with exposure times of 300 s. The $H\alpha$ emission line is strong and has double peaks separated by 750 km s^{-1} (measured from the average spectrum). The HeI 6678 Å line is weaker and its double peaks have a greater separation of 1220 km s^{-1} . The best RV measurements were obtained using the double Gaussian method with FWHMs 300 km s^{-1} and separation 2100 km s^{-1} , giving an orbital period of $P_{\text{orb}} = 113.6 \pm 1.5$ min (Table 3).

The RV curve is not sinusoidal (Fig. 12) and formally the best orbital fit has an eccentricity of $e = 0.09 \pm 0.03$ (giving $\sigma_{\text{rms}} = 11.2$ compared to $\sigma_{\text{rms}} = 12.7$ for a circular orbit) and an orbital period of 113.4 min. It is difficult to find a reason for an interacting close binary star to have an eccentric orbit, and we do not believe that this is the case for SDSS J1642. Many CVs have emission-line RV variations which do not match the motion of the white dwarf component (Stover 1981; Steeghs et al. 2007), and an apparently significant nonzero orbital eccentricity may result from the same distortion mechanisms. We therefore adopt the orbital period from the circular RV orbit, which in this case is

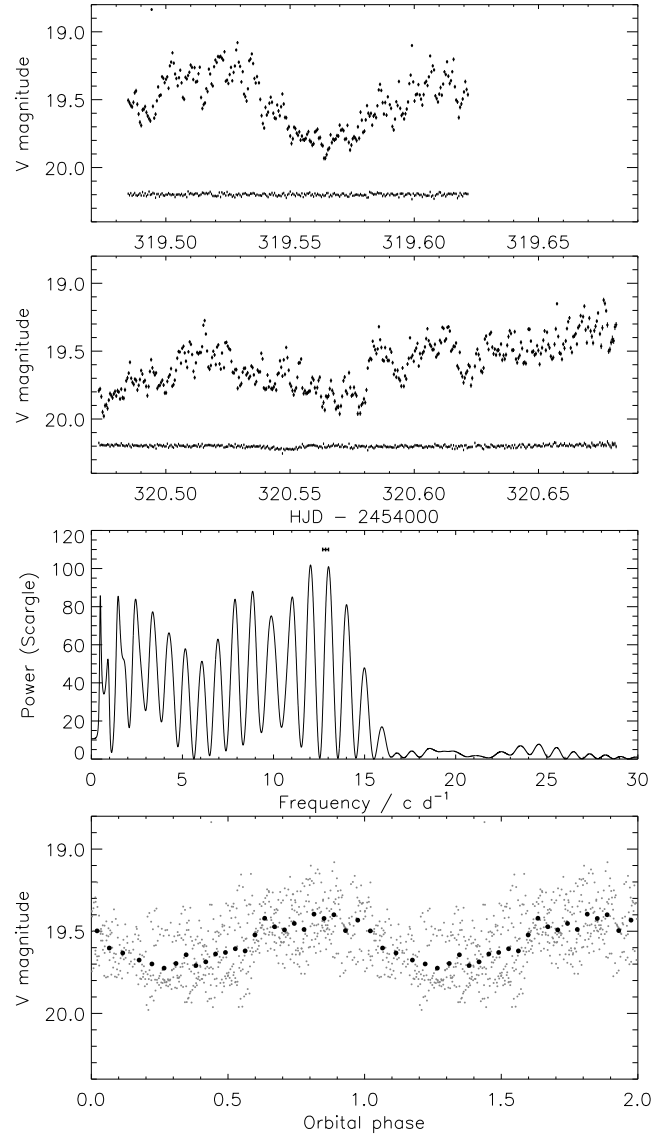


Figure 11. NTT V -filter photometry of SDSS J1642. The upper two panels show the light curves from the individual nights as well as differential photometry between the two comparison stars used (offset to appear in the plot). The third panel shows the Scargle periodogram of the combined data from the two nights, and the spectroscopic orbital period value is indicated at the top of the plot. The bottom panel shows the data phased with the photometric period of 110.6 min (grey dots) and combined into 25 phase bins (black filled circles). In most cases the error bars are smaller than the points.

in excellent agreement with the period from the eccentric-orbit alternative. The spectra have been phase-binned with this period and shown as a trailed greyscale plot in Fig. 3. The emission shows clear double peaks at both $H\alpha$ and HeI 6678 Å.

Using the orbital period we measured from the VLT spectra we can now select the peak(s) in the light curve periodogram which may correspond to this value. The two highest peaks are at periods of 110.6 and 119.7 min (Fig. 11), which agree with the spectroscopic period to within 2σ

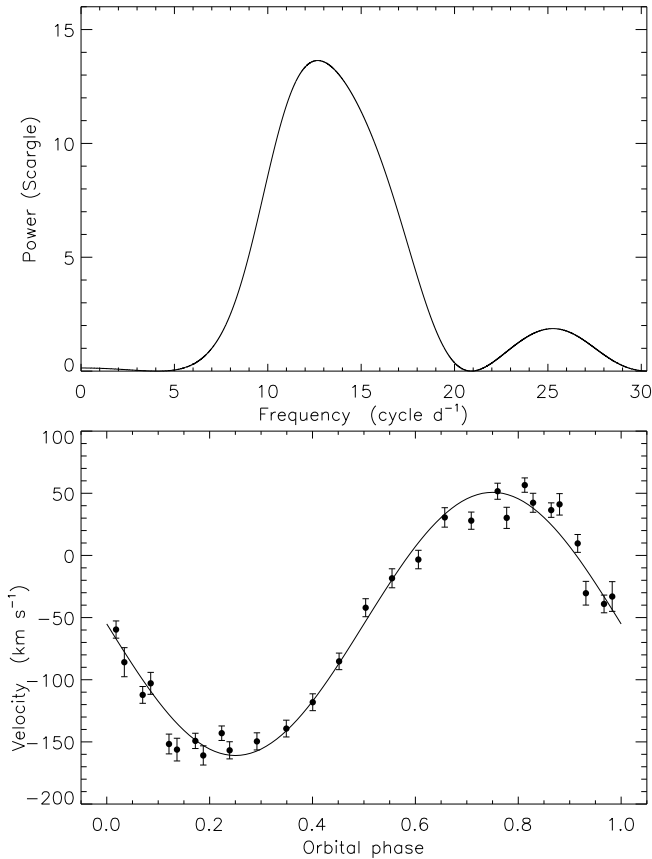


Figure 12. *Upper panel:* Scargle periodogram of the RV of SDSS J1642 measured using a double Gaussian with width 300 km s^{-1} and separation 2100 km s^{-1} . *Lower panel:* measured RVs (filled circles) compared to the best-fitting spectroscopic orbit (solid line).

and 4σ , respectively. The former of these has a period of $110.60 \pm 0.16 \text{ min}$. This might represent the orbital period of the system, but the data in hand are insufficient to be sure. We therefore adopt the spectroscopic value, $P_{\text{orb}} = 113.6 \pm 1.5 \text{ min}$, as the orbital period of SDSS J1642.

4.5.1 Doppler tomography of SDSS J1642

The trailed spectra for SDSS J1642 (Fig. 3) show that the He I 6678 \AA emission line appears to be wider than the $\text{H}\alpha$ line. We have therefore calculated Doppler maps for SDSS J1642, in the same way as for SDSS J0043 (Section 4.1.2), to investigate this further. The maps are plotted in Fig. 13 and indeed show that the accretion disc seems to span a wider range of velocities in He I 6678 \AA and He I 7065 \AA than for $\text{H}\alpha$. These higher velocities imply that the helium emission comes from a physically smaller part of the disc, specifically the hotter annuli closer to the white dwarf surface.

A second feature of the $\text{H}\alpha$ Doppler map (but not the He I maps) is an inner emission feature that, by analogy with SDSS J0043 and many other CVs, can be attributed to the surface of the secondary star. The interpretations of the maps in Fig. 13 assume $K_2 = 350 \text{ km s}^{-1}$ and a phase off-

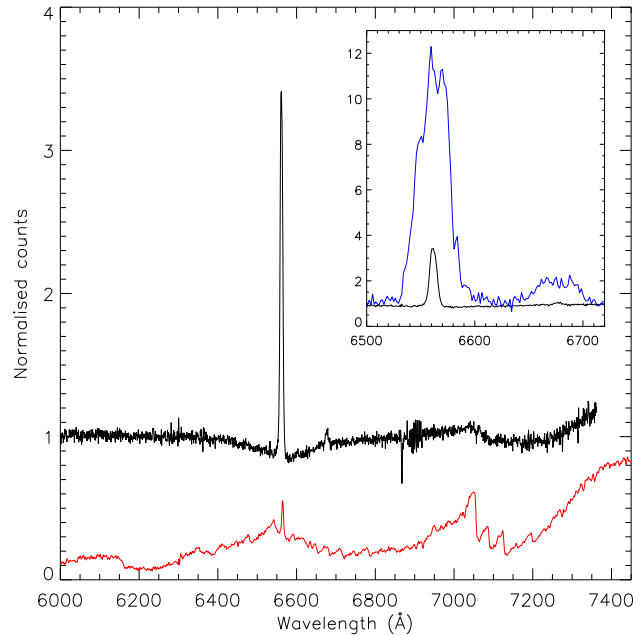


Figure 14. *Main panel:* The mean spectrum of SDSS J1658 from our VLT observations (black line), normalised unity using a straight-line fit. A template M5 star is shown, with a red line, for comparison. *Inset panel:* A comparison between our mean VLT spectrum (black line) and the SDSS spectrum of SDSS J1658 (blue line) in the region of the $\text{H}\alpha$ and He I 6678 \AA lines.

set of 0.15. In this interpretation, the lower velocities of the accretion disc in the $\text{H}\alpha$ map overlap that of the inner emission feature, which violates Kepler’s third law. The disparity between the $\text{H}\alpha$ and He I Doppler maps, and the apparent violation of Kepler’s third law, can both be explained by the breakdown of the assumption that all emitting material is optically thin. If the accretion disc is optically thin to He I emission but partially optically thick for $\text{H}\alpha$, it is quite possible that the detected $\text{H}\alpha$ emission is biased towards lower velocities.

The $\text{H}\alpha$ map also shows a region of strong emission coming from the accretion disc, on the side opposite to the bright spot and reminiscent of the Doppler maps of SDSS J0043 (Section 4.1). Our spectroscopic observations only cover 1.5 orbital periods of this system, and the region of strong emission could be caused by brightness variations which change between different orbits (which is not taken into account when calculating the Doppler maps). Additional observations are needed to further investigate the unusual characteristics of SDSS J1642.

4.6 SDSS J165837.70+184727.4

SDSS J1658 was discovered to be a CV by Szkody et al. (2006) and its SDSS spectrum shows the strong Balmer emission and weaker He I emission lines typical of short-period CVs. The Balmer emission is single-peaked and the He I emission is weakly double-peaked.

We obtained 31 VLT spectra of SDSS J1658 over two consecutive nights in 2007 August. At the times of the SDSS imaging observations and our spectroscopy, the system had

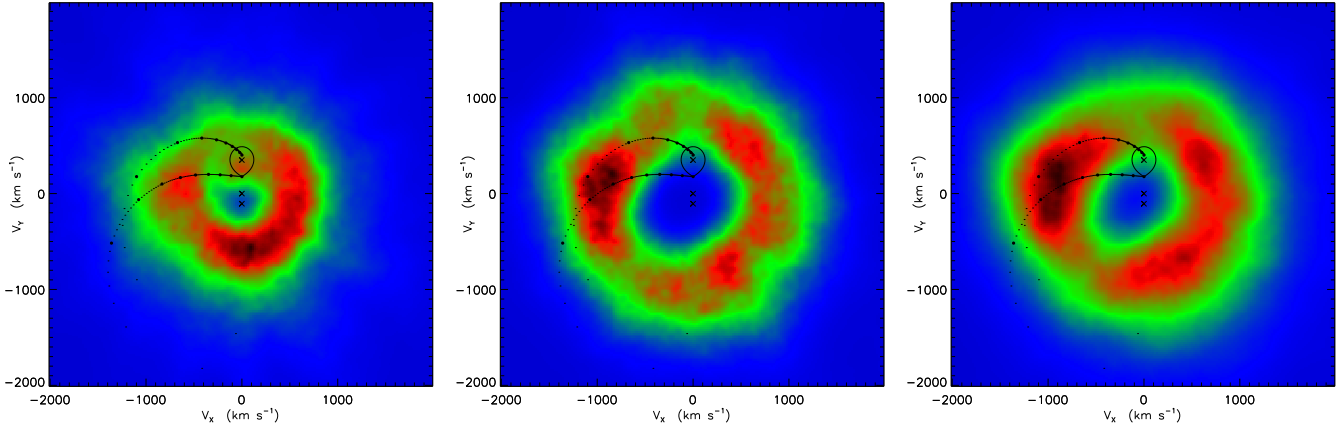


Figure 13. Doppler maps of the H α (left), He I 6678 Å (centre) and He I 7065 Å (right) emission lines from SDSS J1642. The symbols are overlotted in the same way as for Fig. 6.

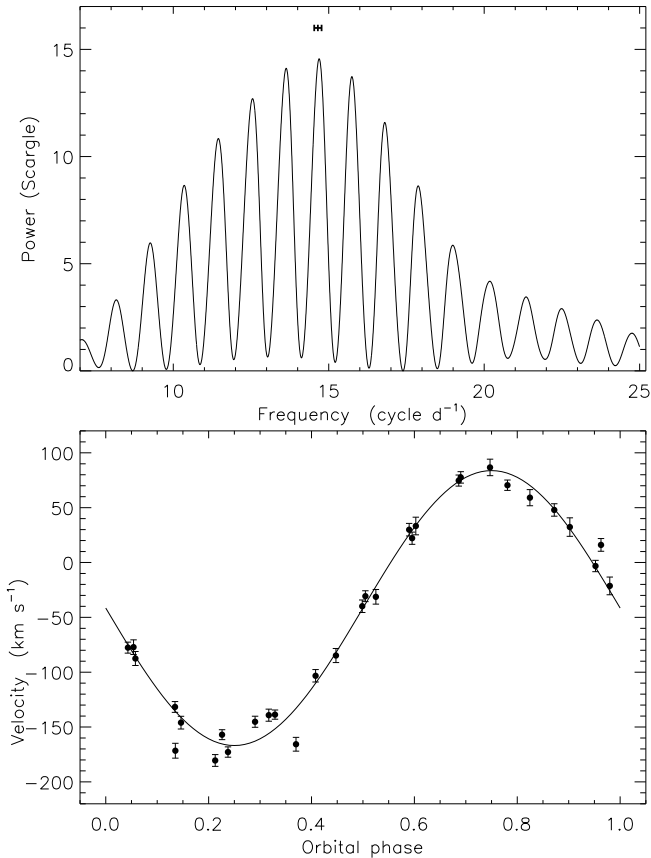


Figure 15. *Upper panel:* Scargle periodogram of the RVs of SDSS J1658 measured using a single Gaussian with width 400 km s^{-1} . *Lower panel:* measured RVs (filled circles) compared to the best-fitting spectroscopic orbit (solid line).

an apparent g or V magnitude of ~ 20 . However, the spectroscopic characteristics of SDSS J1658 are very different in our observations compared to the SDSS spectrum (where it was at magnitude $g_{\text{spec}} = 19.7$). Fig. 14 shows that the emission lines in the SDSS spectrum are remarkably strong and broad (for example, H α has FWHM 35 \AA and equivalent

width 360 \AA) but in the VLT data are extremely weak (7 \AA and 25 \AA , respectively). Spectral features from both stellar components are visible in the mean VLT spectrum: we see a broad H α absorption from the white dwarf photosphere and a wide $7150\text{--}7350 \text{ \AA}$ dip which betrays the presence of an M-type secondary star (Fig. 14).

At the time of the SDSS spectrum SDSS J1658 was clearly in a state of much higher accretion level than during the other observations. This is manifested in the vastly stronger emission lines from the accretion disc, but the disc still contributed very little continuum light so the CV was only slightly brighter at that time. The stellar components are not clearly visible in the SDSS spectrum due to the wider emission lines and much lower S/N than our mean VLT spectrum.

The RV motion of the H α line in our spectra is straightforward to detect. Single-Gaussian measurements were made and the best FWHM was found to be 400 km s^{-1} , giving an orbital period of $98.29 \pm 0.79 \text{ min}$ from 19 spectra on the first night only. Including the spectra from the second night gives the expected alias pattern centred on a period of 98.05 min with one-day aliases at 91.48 and 105.70 min . We can therefore unambiguously identify the central peak in the periodogram with the orbital motion of the binary, resulting in a final period of $P_{\text{orb}} = 98.012 \pm 0.065 \text{ min}$. The spectroscopic orbit is plotted in Fig. 15 and its parameters are given in Table 3.

The velocity amplitude we have measured from the H α emission, $K_1 = 125.3 \pm 3.5 \text{ km s}^{-1}$, is too high to be attributed to the white dwarf, and is far too narrow to arise from the full accretion disc. We therefore tentatively assign it to the secondary star. An additional constraint on the system is that the full width at zero intensity of the H α line in the SDSS spectrum (roughly 3200 km s^{-1}) arises from material in orbit around the white dwarf. We have constructed a constraints diagram in a similar fashion as for SDSS J121607.03+052013.9 (Southworth et al. 2006) and SDSS J013132.39–090122.2 (Southworth et al. 2007b), and required that our measured velocity amplitude is attributable to some part of the secondary star. We find that there is a small region of parameter space where the system could satisfy all our constraints, involving a large white dwarf mass ($1.0 M_{\odot}$ or more) and a low orbital inclination

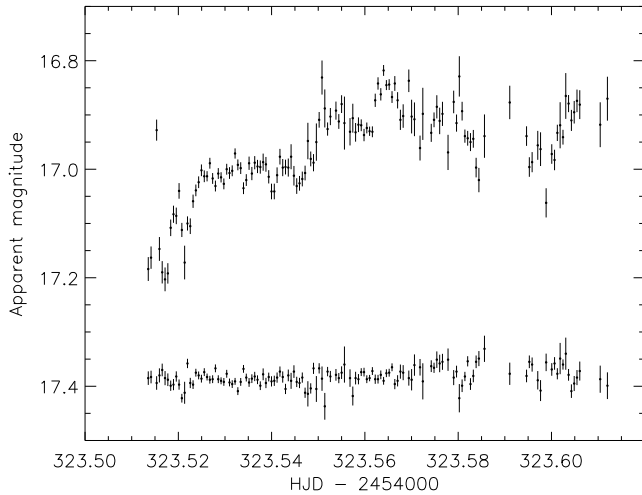


Figure 16. NTT V -filter photometry of SDSS J1659 obtained in cloudy conditions. Differential magnitudes for SDSS J1659 minus comparison star are shown as filled circles with error bars, offset by the V magnitude of the comparison. Differential magnitudes for the comparison minus the check star are shown offset at the bottom of the plot.

($10\text{--}30^\circ$). This solution also allows the secondary star to have a mass near to $0.15 M_\odot$, which is the value expected for a CV with a period of 98 min (Knigge 2006). This is only a rough investigation: more detailed studies would require a more accurate measurement of the emission-line full width at zero intensity when the system is again in the high state. An alternative explanation is that the narrow emission comes from some other structure in the system.

Our VLT data for SDSS J1658 have characteristics reminiscent of the spectrum of the low-inclination CV RE J1255+266 presented by Watson et al. (1996), which shows wide absorption from the white dwarf and very narrow Balmer emission. In the case of RE J1255+266, the narrow emission arises from the accretion disc and has a much lower velocity amplitude than the one we measure for SDSS J1658.

4.7 SDSS J165951.68+192745.6

SDSS J1659 was found to be a CV by Szkody et al. (2006) from an SDSS spectrum which has the extremely blue continuum and weak single-peaked emission lines which are characteristic of a high mass transfer rate (e.g. Rodríguez-Gil et al. 2007a and Rodríguez-Gil et al. 2007b). We obtained 2.5 hours of V -filter NTT photometry of SDSS J1659 (Fig. 16) as a brighter ($g = 17.12$) backup target during cloudy conditions. There is flickering (Bruch 1992, 2000) but no clear coherent periodicity in these data.

4.8 SDSS J223252.35+140353.0

SDSS J2232 was found at magnitude $g = 17.7$ by the SDSS imaging survey. It was subsequently selected for spectroscopic follow-up, and the SDSS spectrum (Szkody et al. 2004) shows Balmer emission lines emanating from a much fainter object ($g_{\text{spec}} = 23.2$). This indicates that SDSS J2232 is a dwarf nova which was in outburst at the time of the

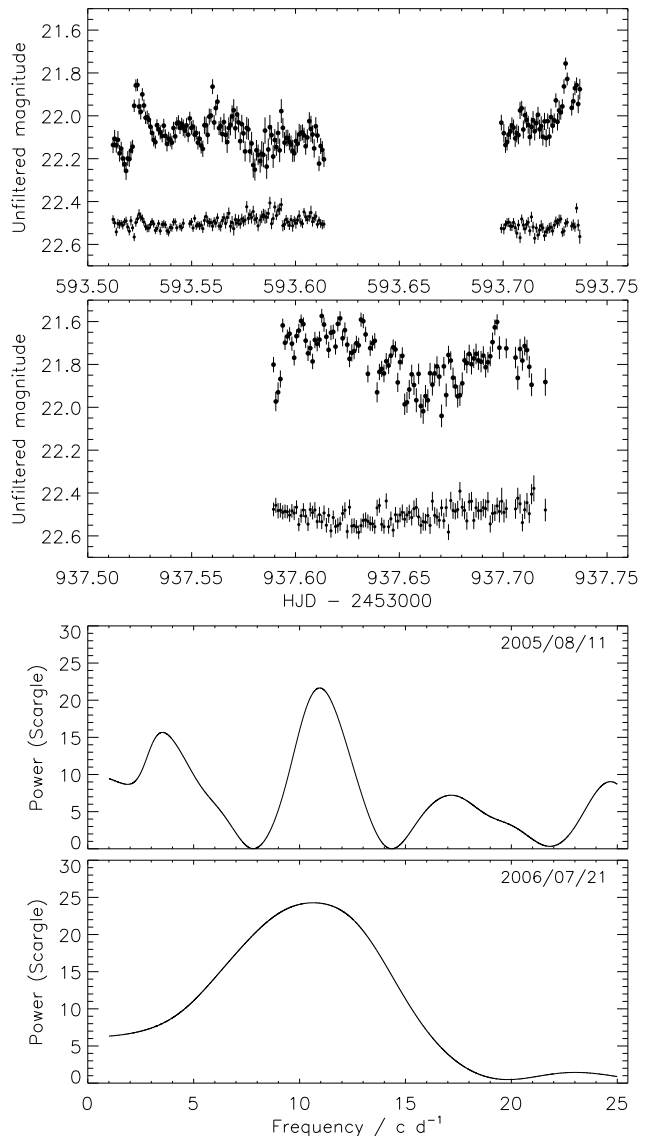


Figure 17. Upper panels: NOT unfiltered light curves of SDSS J2232. The comparison minus check magnitudes are shown in each panel offset to a magnitude of 20.4. Lower panels: Scargle periodograms of the two light curves.

SDSS imaging observations but in quiescence during the SDSS spectroscopic observation. On our VLT acquisition image SDSS J2232 was in quiescence at a magnitude of $V = 21.4$, whereas it was at magnitudes 22.1 and 21.8 during our visits to it with the NOT.

The NOT light curves cover time intervals of about three and five hours, separated by slightly less than one year. Both show a variation with a period in the region of 135 min. The light curves and Scargle periodograms are shown in Fig. 17. Fitting sine curves to the data results in periods of 131 ± 3 min for the 2005 data and 132 ± 6 min for the 2006 observations. With the VLT we obtained 14 $H\alpha$ spectra over 2.5 hours, but then discontinued our observations for scheduling reasons. The resulting RVs (Fig. 18) are consistent with orbital motion with a period longer than 4 hours.

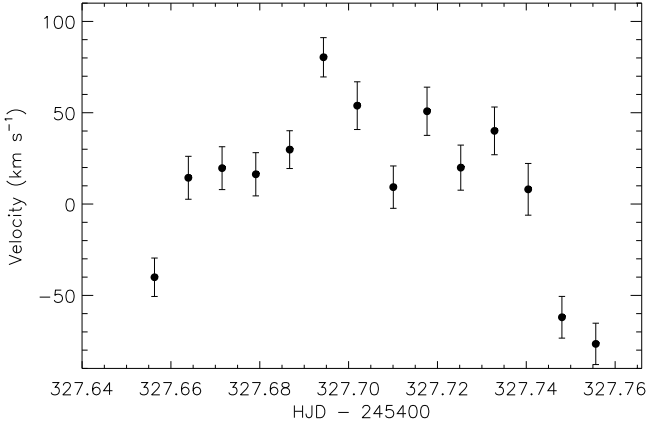


Figure 18. RVs measured for SDSS J2232 using a double Gaussian function with FWHMs 500 km s^{-1} and separation 2000 km s^{-1} .

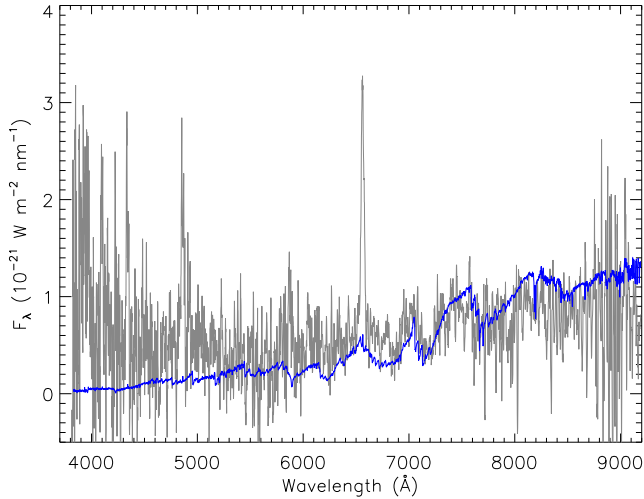


Figure 19. Comparison between the SDSS spectrum of SDSS J2232 (grey line; the data have been smoothed) and a template SDSS spectrum of an M4 dwarf (blue line).

The SDSS spectrum of SDSS J2232 has a very low signal but has a significant contribution from the secondary star. A simple fit to the SDSS spectrum (see Southworth et al. 2006) indicates a secondary component with a spectral type of M4 and a magnitude $r = 23.4$ (Fig. 19). We would therefore expect to see an ellipsoidal modulation in the light curve of this system, with a period of half of the orbital period. The observed periodicity of roughly 135 min implies an orbital period of about 270 min, consistent with the RVs measured from our VLT spectra. We therefore suggest that SDSS J2232 is a dwarf nova with $P_{\text{orb}} \sim 4.5 \text{ hr}$. These properties are similar to those of the well-studied dwarf novae U Gem ($P_{\text{orb}} = 254.7 \text{ min}$ and secondary spectral type $\sim \text{M4}$; Naylor et al. 2005; Echevarría et al. 2007) and GY Cnc (252.6 min and M3; Gänsicke et al. 2000; Thorstensen 2000).

The distance to this system can be estimated using Roche geometry. Assuming $M_{\text{WD}} = 0.6$ and $q = 0.5$ gives a

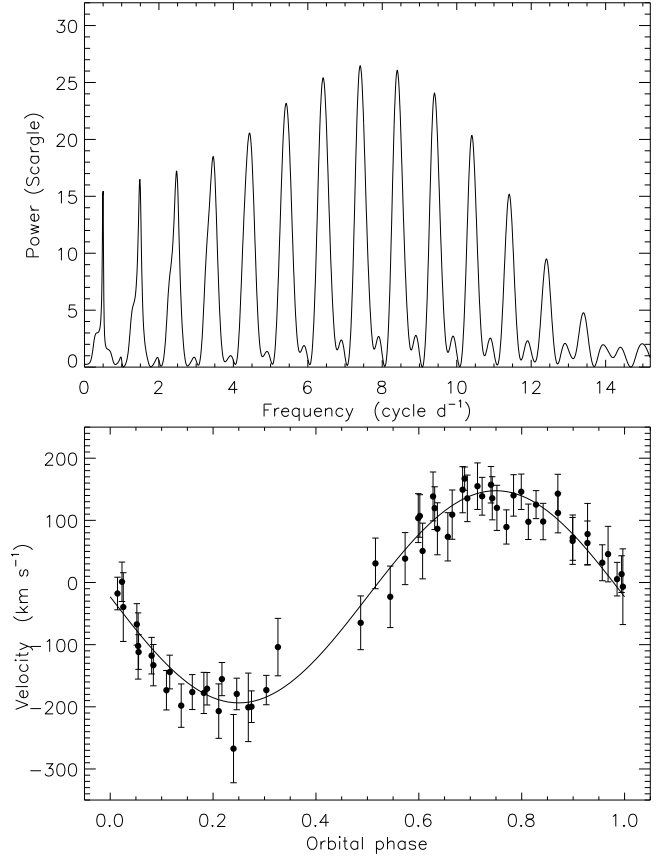


Figure 20. *Upper panel:* Scargle periodogram of the RVs of SDSS J2238 measured using a single Gaussian with FWHM 850 km s^{-1} . *Lower panel:* measured RVs (filled circles) compared to the best-fitting spectroscopic orbit (solid line).

secondary star radius of about $2.5 \times 10^8 \text{ m}$. Accounting for the flux ratio between the SDSS spectrum of SDSS J2232 and a template M4 dwarf spectrum (and the flux from the white dwarf and the accretion disc), we find a distance of about 2.7 kpc. Alternatively, adopting a secondary spectral type of M4 gives an absolute visual magnitude of $M_V = 11.3$. The SDSS magnitude $r = 23.4$ converts to $V = 24.0$, which then results in a distance of roughly 3.5 kpc. A distance of approximately 3 kpc puts SDSS J2232 about 2 kpc from the Galactic plane. This is well into the Galactic thick disc, which has a scale height close to 1 kpc (Veltz et al. 2008). Further observations to assess the membership of SDSS J2232 in this old stellar population may be very rewarding.

4.9 SDSS J223843.84+010820.7 (Aqr 1)

SDSS J2238 was found to be a CV by Berg et al. (1992) in the course of the Large Bright Quasar Survey (Foltz et al. 1987). It was given the provisional name of Aqr 1 in the now-frozen catalogue of Downes et al. (2001). An SDSS spectrum was presented by Szkody et al. (2003), along with seven intermediate-resolution spectra and 3.75 hours of unfiltered time-series photometry with exposure times of 600 s. An orbital period of $\sim 2 \text{ h}$ was estimated from the spectra (al-

Table 4. Summary of the orbital periods obtained for the objects studied in this work.

Object	Period (min)	Notes
SDSS J0043	82.325 ± 0.088	VLT spectroscopy
SDSS J0337		Faint, no RV motion noticed
SDSS J1601	short period	More photometry needed
SDSS J1637	97.04 ± 0.19	VLT spectroscopy
SDSS J1642	113.6 ± 1.5	VLT spectroscopy
SDSS J1658	98.012 ± 0.065	VLT spectroscopy, low state
SDSS J1659		NTT photometry
SDSS J2232		VLT spec., period may be ~ 4.5 hr
SDSS J2238	194.30 ± 0.16	Magellan spectroscopy

though they only cover 1.75 h), and no periodic variation was noticed in the photometry. The He II 4686 Å emission in the SDSS spectrum was strong enough for Szkody et al. (2003) to suggest that the object may be a magnetic CV.

Woudt et al. (2004) presented 15 h of unfiltered photometry of SDSS J2238 over five nights, obtained using the SAAO 1.9 m telescope and UCT high-speed photometer. They found periodicities at 6.7284 min and 193.5 min, the second of which was found to be the ‘probable’ orbital period. The first of these was attributed to the spin period of the white dwarf, confirming the magnetic nature of the object.

We obtained a total of 59 spectra over three consecutive nights (Table 2) using the IMACS spectrograph on the Magellan Baade telescope (Section 2.3). RV measurements of the H α line indicate an orbital period of 194 min for all widths of Gaussian functions tried. The best results are found using a single Gaussian of width 850 km s^{-1} . A Scargle periodogram of these observations is highly aliased (Fig. 20) but bootstrapping simulations give a probability of 88% that the highest peak is the correct one. Fitting a spectroscopic orbit to the RVs gives an orbital period of $P_{\text{orb}} = 194.30 \pm 0.16$ min. Whilst this solution gives a scatter in the observations of $\sigma_{\text{rms}} = 27.3 \text{ km s}^{-1}$, the alternative alias periods of 171 and 224 min have scatter of 35.0 and 34.1 km s^{-1} , respectively.

Our orbital period of 194.30 min is in good agreement with the ‘probable orbital period’ obtained by Woudt et al. (2004), which supports both our alias discrimination and their interpretation. The discrepant value of ~ 2 h favoured by Szkody et al. (2003) is probably due to the shortage of observational data available to that study. The parameters of the final spectroscopic orbit are given in Table 3 and phase-binned and trailed spectra around the H α and He I 6678 Å emission lines are shown in Fig. 3. The 6.7 min photometric periodicity found by Woudt et al. (2004) is not resolved by our spectra, which have a cadence of 5.5 min.

5 SUMMARY AND DISCUSSION

We have presented time-resolved photometry and spectroscopy of nine faint CVs which were identified by the SDSS. For five of these systems we have determined orbital periods (Table 4), and four of these are shorter than the 2–3 hour period gap apparent in the known population of

CVs. This work brings the total number of SDSS CVs with measured orbital periods to approximately 110 of the total population of 212 objects.

From VLT spectroscopy of SDSS J0043 we found an orbital period of $P_{\text{orb}} = 82.325 \pm 0.088$ min, placing this object close to the observed minimum period for hydrogen-rich CVs. Its spectrum shows a strong contribution from the white dwarf in the system, indicating that the accretion disc is faint and the mass transfer rate is low. We have used Doppler tomography to decompose the spectra into a Doppler map in velocity space. The map shows a circular accretion disc and an inner emission peak. The latter feature can be attributed to the irradiated inner face of the secondary star, if the velocity amplitude measured from the H α emission line overestimates the motion of the white dwarf by a factor of two. The Doppler map shows enhanced emission from two bright regions on the accretion disc. If the inner emission peak does indeed come from the secondary star, one of these bright regions is in the correct position to be a bright spot caused by the mass transfer stream impacting the disc. This interpretation is supported by its presence in a Doppler map of the He I 6678 Å line. The second region of enhanced emission is in an unusual position in velocity space and its origin is not straightforwardly explicable. A short light curve of SDSS J0043 shows evidence of a variation with a period of 207 ± 1 s and an amplitude of 17 ± 5 mmag. The white dwarf component may be a ZZ Ceti-type pulsating star.

SDSS J1637 was observed with the VLT during quiescence, resulting in an orbital period measurement of $P_{\text{orb}} = 97.01 \pm 0.19$ min. This object is a dwarf nova which has previously been observed in superoutburst, when superhumps with a period of 99.75 ± 0.86 min were detected. Using the calibrations presented by Patterson (1998) and Knigge (2006), we find $q \approx 0.16$ from these two period measurements. Assuming a white dwarf mass of $0.8 M_{\odot}$ gives an estimated secondary mass of $0.13 M_{\odot}$. This is in good agreement with the expected properties of a CV with $P_{\text{orb}} = 97$ min, and together with the velocity amplitude from the H α emission line point to the system having an orbital inclination of roughly 40° .

SDSS J1642 was studied both photometrically with the NTT and spectroscopically with the VLT. The VLT data yield an unambiguous period of $P_{\text{orb}} = 113.6 \pm 1.5$ min. The NTT photometry shows a number of features and results in a periodogram with a small forest of peaks at frequencies below 15 cycle d^{-1} . The spectroscopic period is in best agreement with the peak corresponding to a period of 110.60 ± 0.16 min, but we prefer the spectroscopic value for our final orbital period measurement. Doppler maps of the H α and He I emission lines reveal a clear accretion disc and bright spot as well as weak emission from the secondary star. More surprisingly, the He I maps show an accretion disc with much higher velocities than those for H α , indicating that the emitting region for He I is physically smaller and closer to the white dwarf than for H α . The H α map also shows strong emission arising from the part of the disc opposite the bright spot, but the short duration of our spectroscopic observations means this unusual feature could be caused by brightness variation which differ from orbit to orbit.

SDSS J1658 is perhaps the most unusual system studied in this work. Its SDSS spectrum shows the strong emission lines characteristic of a short-period CV whose light is dom-

inated by a hydrogen-rich accretion disc. However, our VLT spectra show a much weaker and narrower central emission line, and broad absorption features arising from both the white dwarf and secondary star, but no flux which could be unambiguously assigned to an accretion disc. The object was only 0.4 mag fainter during our observations than when the SDSS spectrum was taken, so the strong emission lines in that spectrum were accompanied by only weak continuum flux from the accretion disc. The velocity variation of the narrow H α emission in our VLT spectra yields a period measurement of $P_{\text{orb}} = 98.012 \pm 0.065$ min, confirming that this object is a short-period binary star system. The velocity amplitude (125 km s^{-1}) is too large for the white dwarf, so we have attempted to assign it to the secondary star. The observational constraints can be satisfied in this scenario if the white dwarf is massive ($\lesssim 1 M_{\odot}$) and the orbital inclination is low ($10\text{--}30^{\circ}$).

A modest number of photometric and spectroscopic observations of SDSS J2232 suggest that this is a dwarf nova with an orbital period close to 4.5 hr. From the flux contribution of the secondary star we infer a distance of roughly 3 kpc, corresponding to distance of 2 pkc from the Galactic plane. Further investigation is needed to prove its membership of this old stellar population.

We obtained 59 Magellan spectra of SDSS J2238, which is the brightest of the five objects for which we determine orbital periods in this work. Velocity measurements of its H α emission line give a period of $P_{\text{orb}} = 194.30 \pm 0.16$. This value is in good agreement with a published photometric period, which also confirmed that the system contains a magnetic white dwarf with a rotational period of 6.7284 min.

These observations provide further confirmation that the faintest of the CVs identified by the SDSS have predominantly short orbital periods. Theoretical population studies of CVs predict a huge population of faint short-period CVs which has not previously been detected. Our observations are now uncovering this ‘quiet majority’ of the CV population. The unusual characteristics of several of the objects studied in this work show that even the short-period CVs demonstrate impressively varied behaviour, many aspects of which cannot easily be explained in the standard picture of CV structure. Our project to study the SDSS CV population is invaluable for extending our knowledge of these fascinating objects.

ACKNOWLEDGEMENTS

The reduced spectra and radial velocity measurements presented in this work will be made available at the CDS (<http://cdsweb.u-strasbg.fr/>) and at <http://www.astro.keele.ac.uk/~jkt/>. Based on observations made with ESO Telescopes at the La Silla and Paranal Observatories under programme ID 079.D-0024. Some data presented here have been taken using ALFOSC, which is owned by the Instituto de Astrofísica de Andalucía (IAA) and operated at the Nordic Optical Telescope under agreement between IAA and the NBIfAFG of the Astronomical Observatory of Copenhagen.

We would like to acknowledge the referee, John Thorstensen, for an insightful report. JS and CMC acknowledge financial support from PPARC in the form of a post-

doctoral research assistant position. DS acknowledges an STFC Advanced Fellowship. The following internet-based resources were used in research for this paper: the ESO Digitised Sky Survey; the NASA Astrophysics Data System; the SIMBAD database operated at CDS, Strasbourg, France; and the arXiv scientific paper preprint service operated by Cornell University.

Funding for the Sloan Digital Sky Survey (SDSS) has been provided by the Alfred P. Sloan Foundation, the Participating Institutions, the National Aeronautics and Space Administration, the National Science Foundation, the U. S. Department of Energy, the Japanese Monbukagakusho, and the Max Planck Society. The SDSS website is <http://www.sdss.org/>.

REFERENCES

- Appenzeller, I., et al., 1998, *The Messenger*, 94, 1
 Aungwerojwit, A., et al., 2006, *A&A*, 455, 659
 Berg, C., Wegner, G., Foltz, C. B., Chaffee, Jr., F. H., Hewett, P. C., 1992, *ApJS*, 78, 409
 Bertin, E., Arnouts, S., 1996, *A&AS*, 117, 393
 Bigelow, B. C., Dressler, A. M., 2003, in Iye, M., Moorwood, A. F. M., eds., *Instrument Design and Performance for Optical/Infrared Ground-based Telescopes*. Edited by Iye, Masanori; Moorwood, Alan F. M. *Proceedings of the SPIE*, Volume 4841, pp. 1727-1738 (2003)., vol. 4841 of *Presented at the Society of Photo-Optical Instrumentation Engineers (SPIE) Conference*, p. 1727
 Bruch, A., 1992, *A&A*, 266, 237
 Bruch, A., 2000, *A&A*, 359, 998
 Chen, A., O’Donoghue, D., Stobie, R. S., Kilkenny, D., Warner, B., 2001, *MNRAS*, 325, 89
 de Kool, M., 1992, *A&A*, 261, 188
 de Kool, M., Ritter, H., 1993, *A&A*, 267, 397
 Dillon, M., et al., 2008a, *MNRAS*, 386, 1568
 Dillon, M., et al., 2008b, *MNRAS*, in preparation
 D’Odorico, S., Beletic, J. W., Amico, P., Hook, I., Marconi, G., Pedichini, F., 1998, in D’Odorico, S., ed., *Proc. SPIE Vol. 3355, Optical Astronomical Instrumentation*, vol. 3355 of *Society of Photo-Optical Instrumentation Engineers (SPIE) Conference*, p. 507
 Downes, R. A., Webbink, R. F., Shara, M. M., Ritter, H., Kolb, U., Duerbeck, H. W., 2001, *PASP*, 113, 764
 Eaton, N., Draper, P. W., Allen, A., 1999, *Starlink User Note* 45.9
 Echevarría, J., de la Fuente, E., Costero, R., 2007, *AJ*, 134, 262
 Foltz, C. B., Chaffee, Jr., F. H., Hewett, P. C., MacAlpine, G. M., Turnshek, D. A., Weymann, R. J., Anderson, S. F., 1987, *AJ*, 94, 1423
 Gänsicke, B. T., Fried, R. E., Hagen, H.-J., Beuermann, K., Engels, D., Hessman, F. V., Nogami, D., Reinsch, K., 2000, *A&A*, 356, L79
 Gänsicke, B. T., Araujo-Betancor, S., Hagen, H.-J., Harlaftis, E. T., Kitsionas, S., Dreizler, S., Engels, D., 2004, *A&A*, 418, 265
 Gänsicke, B. T., et al., 2006, *MNRAS*, 365, 969
 Green, R. F., Schmidt, M., Liebert, J., 1986, *ApJS*, 61, 305

- Hellier, C., 2001, *Cataclysmic Variable Stars: How and Why they Vary*, Springer-Praxis books in astronomy and space science, Springer Verlag, New York
- Horne, K., 1986, *PASP*, 98, 609
- Howell, S. B., Nelson, L. A., Rappaport, S., 2001, *ApJ*, 550, 897
- Jester, S., et al., 2005, *AJ*, 130, 873
- Knigge, C., 2006, *MNRAS*, 373, 484
- Kolb, U., 1993, *A&A*, 271, 149
- Kolb, U., Baraffe, I., 1999, *MNRAS*, 309, 1034
- Kolb, U., de Kool, M., 1993, *A&A*, 279, L5
- Littlefair, S. P., Dhillon, V. S., Marsh, T. R., Gänsicke, B. T., 2006a, *MNRAS*, 371, 1435
- Littlefair, S. P., Dhillon, V. S., Marsh, T. R., Gänsicke, B. T., Southworth, J., Watson, C. A., 2006b, *Science*, 314, 1578
- Littlefair, S. P., Dhillon, V. S., Marsh, T. R., Gänsicke, B. T., Baraffe, I., Watson, C. A., 2007, *MNRAS*, 381, 827
- Littlefair, S. P., et al., 2008, *MNRAS*, in press
- Marsh, T. R., 1989, *PASP*, 101, 1032
- Marsh, T. R., Horne, K., 1988, *MNRAS*, 235, 269
- Mukadam, A. S., et al., 2004, *ApJ*, 607, 982
- Naylor, T., 1998, *MNRAS*, 296, 339
- Naylor, T., Allan, A., Long, K. S., 2005, *MNRAS*, 361, 1091
- O'Donoghue, D., Kanaan, A., Kleinman, S. J., Krzesinski, J., Pritchett, C., 2000, *Baltic Astronomy*, 9, 375
- Osterbrock, D. E., Fulbright, J. P., Martel, A. R., Keane, M. J., Trager, S. C., Basri, G., 1996, *PASP*, 108, 277
- Paczynski, B., 1967, *Acta Astronomica*, 17, 287
- Patterson, J., 1998, *PASP*, 110, 1132
- Politano, M., 1996, *ApJ*, 465, 338
- Politano, M., 2004, *ApJ*, 604, 817
- Press, W. H., Teukolsky, S. A., Vetterling, W. T., Flannery, B. P., 1992, *Numerical recipes in FORTRAN 77. The art of scientific computing*, Cambridge: University Press, 2nd ed.
- Rappaport, S., Joss, P. C., Webbink, R. F., 1982, *ApJ*, 254, 616
- Ritter, H., Kolb, U., 2003, *A&A*, 404, 301
- Rodríguez-Gil, P., Schmidtobreick, L., Gänsicke, B. T., 2007a, *MNRAS*, 374, 1359
- Rodríguez-Gil, P., et al., 2007b, *MNRAS*, 377, 1747
- Roelofs, G. H. A., Groot, P. J., Marsh, T. R., Steeghs, D., Nelemans, G., 2006, *MNRAS*, 365, 1109
- Scargle, J. D., 1982, *ApJ*, 263, 835
- Schneider, D. P., Young, P., 1980, *ApJ*, 238, 946
- Schwarzenberg-Czerny, A., 1989, *MNRAS*, 241, 153
- Schwarzenberg-Czerny, A., 1996, *ApJ*, 460, L107
- Shafter, A. W., 1983, *ApJ*, 267, 222
- Smak, J., 1985, *Acta Astronomica*, 35, 351
- Smith, D. A., Dhillon, V. S., 1998, *MNRAS*, 301, 767
- Southworth, J., Maxted, P. F. L., Smalley, B., 2004a, *MNRAS*, 349, 547
- Southworth, J., Maxted, P. F. L., Smalley, B., 2004b, *MNRAS*, 351, 1277
- Southworth, J., Zucker, S., Maxted, P. F. L., Smalley, B., 2004c, *MNRAS*, 355, 986
- Southworth, J., Smalley, B., Maxted, P. F. L., Claret, A., Etzel, P. B., 2005, *MNRAS*, 363, 529
- Southworth, J., Gänsicke, B. T., Marsh, T. R., de Martino, D., Hakala, P., Littlefair, S., Rodríguez-Gil, P., Szkody, P., 2006, *MNRAS*, 373, 687 (Paper I)
- Southworth, J., Gänsicke, B. T., Marsh, T. R., de Martino, D., Aungwerojwit, A., 2007a, *MNRAS*, 378, 635
- Southworth, J., Marsh, T. R., Gänsicke, B. T., Aungwerojwit, A., Hakala, P., de Martino, D., Lehto, H., 2007b, *MNRAS*, 382, 1145
- Southworth, J., Townsley, D. M., Gänsicke, B. T., 2008, *MNRAS*, 388, 709
- Spruit, H. C., Ritter, H., 1983, *A&A*, 124, 267
- Steeeghs, D., Howell, S. B., Knigge, C., Gänsicke, B. T., Sion, E. M., Welsh, W. F., 2007, *ApJ*, 667, 442
- Stover, R. J., 1981, *ApJ*, 249, 673
- Szkody, P., et al., 2002, *AJ*, 123, 430
- Szkody, P., et al., 2003, *AJ*, 126, 1499
- Szkody, P., et al., 2004, *AJ*, 128, 1882
- Szkody, P., et al., 2005, *AJ*, 129, 2386
- Szkody, P., et al., 2006, *AJ*, 131, 973
- Szkody, P., et al., 2007, *AJ*, 134, 185
- Thorstensen, J. R., 2000, *PASP*, 112, 1269
- Veltz, L., et al., 2008, *A&A*, 480, 753
- Verbunt, F., Zwaan, C., 1981, *A&A*, 100, L7
- Vogt, N., 1982, *ApJ*, 252, 653
- Warner, B., 1995, *Cataclysmic Variable Stars*, Cambridge Astrophysics Series, Cambridge University Press, Cambridge, UK
- Watson, M. G., Marsh, T. R., Fender, R. P., Barstow, M. A., Still, M., Page, M., Dhillon, V. S., Beardmore, A. P., 1996, *MNRAS*, 281, 1016
- Whitehurst, R., 1988, *MNRAS*, 232, 35
- Whyte, C. A., Eggleton, P. P., 1980, *MNRAS*, 190, 801
- Willems, B., Kolb, U., Sandquist, E. L., Taam, R. E., Dubus, G., 2005, *ApJ*, 635, 1263
- Winget, D. E., 1998, *Journal of Physics Condensed Matter*, 10, 11247
- Woudt, P. A., Warner, B., Pretorius, M. L., 2004, *MNRAS*, 351, 1015
- York, D. G., et al., 2000, *AJ*, 120, 1579